

CONSTRAINING STELLAR PROPERTIES OF INTERVENING DAMPED Ly α AND Mg II ABSORBING GALAXIES TOWARD GRB 050730

Y. MINOWA¹, K. OKOSHI², N. KOBAYASHI³, AND H. TAKAMI⁴

Accepted for publication in The Astronomical Journal

ABSTRACT

We performed multi-band deep imaging of the field around GRB 050730 to identify the host galaxies of intervening absorbers, which consist of a damped Ly α absorption (DLA) system at $z_{\text{abs}} = 3.564$, a sub-DLA system at $z_{\text{abs}} = 3.022$, and strong Mg II absorption systems at $z_{\text{abs}} = 1.773$ and 2.253 . Our observations were performed after the gamma-ray burst afterglow had disappeared. Thus, our imaging survey has a higher sensitivity to the host galaxies of the intervening absorbers than the normal imaging surveys in the direction of QSOs, for which the QSO glare tends to hide the foreground galaxies. In this deep imaging survey, we could not detect any unambiguous candidates for the host galaxies of the intervening absorbers. Using the 3- σ upper limit of the flux in the optical to mid-infrared observing bands, which corresponds to the UV to optical bands in the rest-frame of the intervening absorbers, we constrained the star-formation rates and stellar masses of the hosts. We estimated the star-formation rates for the intervening absorbers as $\lesssim 2.5 M_{\odot} \text{ yr}^{-1}$ for $z > 3$ DLAs and $\lesssim 1.0 M_{\odot} \text{ yr}^{-1}$ for $z \sim 2$ Mg II systems. Their stellar masses are estimated to be several times $10^9 M_{\odot}$ or smaller for all intervening galaxies. These properties are comparable to dwarf galaxies, rather than the massive star-forming galaxies commonly seen in the $z > 2$ galaxy surveys based on emission-line selection or color selection.

Keywords: galaxies: evolution - galaxies: ISM - galaxies: stellar content - gamma-ray burst: individual: (GRB 050730)

1. INTRODUCTION

Exchange of gas and metals between the intergalactic medium and galaxies is a fundamental process of galaxy formation and evolution. In the standard model of galaxy formation based on the cold dark matter (CDM) cosmology (e.g., White & Rees 1978; Fall & Efstathiou 1980), galaxies are thought to be formed by star formation caused by the cooling and condensation of gas in the core of galactic halos produced by the hierarchical clustering of dark matter. To reveal the process of galaxy formation and evolution, it is important to explore the gaseous and stellar properties of young galaxies at high redshifts. The study of stellar populations in high-redshift ($z > 2$) galaxies has been largely developed by the detection of color-selected galaxies, such as Lyman break galaxies (LBGs; Steidel et al. 2003), or emission-line selected galaxies, such as Ly α emitters (LAEs; Cowie & Hu 1998). The study of these galaxy populations provides us with the properties of their stellar population, including star formation rate (SFR), stellar mass, and age. The gaseous properties of high-redshift galaxies, such as hydrogen and metal abundances, have also been studied in this decade, but these studies are mostly based on observations of intergalactic matter identified as hydrogen or metal absorption lines in the spectra of bright QSOs. It is difficult to connect the stellar properties of the emission-line selected galaxies to the gaseous properties of the absorption-line selected galaxies, as they have very different selection biases. The emission-selected samples are biased by their flux and depend on the depth of the imaging

surveys. Therefore, they only provide information in galaxies at the brightest end of the luminosity function. In contrast, the absorption-selected samples are selected homogeneously by their gas content, and thus, they are less biased by the flux of the host galaxies. To connect stellar and gaseous properties of high-redshift galaxies, it is essential to detect the emission line systems.

Among the several absorption lines seen in the spectra of background QSOs, the damped Ly α absorption (DLA) systems (Wolfe et al. 1986) present unique opportunities to select H I-rich (H I column density ($N_{\text{HI}} \geq 10^{20.3} \text{ cm}^{-2}$) galaxies at high redshift. The DLAs dominate the H I content of the universe at $z > 2$ (e.g., Péroux et al. 2003; Prochaska & Wolfe 2009; Noterdaeme et al. 2009) and contain a large amount of H I gas mass, accounting for a large fraction of the present-day stellar mass (Cole et al. 2001). Thus, the high- z galaxies associated with absorbers such as DLAs are expected to be progenitors of present-day galaxies. Many attempts to identify DLA host galaxies have been made so far. At low redshift ($z \leq 1$), a few dozen DLA absorbing galaxies have been established (e.g., Rao et al. 2003; Chen & Lanzetta 2003; Rao et al. 2011), although more than 50% of the known low-redshift DLAs remain unidentified. At high redshift ($z \geq 1$), however, the success rate for discovering DLA host galaxies is quite low, especially at $z > 2$. Only a few DLA host galaxies have been identified (e.g., Møller et al. 2002, 2004; Péroux et al. 2012). This low discovery rate could be caused by the fact that most DLA host galaxies are faint and compact. The glare of the background QSOs also severely hampers the detection of the faint stellar emission from the DLAs. Some independent theoretical predictions suggest that DLA host galaxies have typical luminosities of sub- L_* with a typical proper size of ~ 3 kpc, and 60%-90% of them could be hidden by the glare of bright QSOs (e.g., Fynbo et al. 1999; Okoshi & Nagashima 2005). The limited sample size of iden-

¹ Subaru Telescope, National Astronomical Observatory of Japan, 650 North A'ohoku Place, Hilo, HI 96720, USA minoways@subaru.naoj.org

² Faculty of Industrial Science and Technology, Tokyo University of Science, 102-1 Tomino, Oshamambe, Hokkaido, 049-3514, Japan

³ Institute of Astronomy, School of Science, University of Tokyo, 2-21-1 Osawa, Mitaka, Tokyo 181-0015, Japan

⁴ Optical and Infrared Astronomy Division, National Astronomical Observatory of Japan, 2-21-1 Osawa, Mitaka, Tokyo 181-8588, Japan

tified galaxies associated with DLAs prevents us from continuing investigations to connect the stellar and gaseous properties of high-redshift galaxies. Recently, Fynbo et al. (2010) have initiated an emission-line survey for metal-rich DLAs whose luminosities are expected to be brighter than typical less metal-rich DLAs (Møller et al. 2004; Ledoux et al. 2006). They successfully identified three DLA host galaxies at $z > 2$ in nebular emission (Fynbo et al. 2010, 2011; Noterdaeme et al. 2012). As for typical less metal-rich DLA host galaxies, only a few have been successfully detected to date. Even in the cases of the identified DLA host galaxies, the contamination from the QSO light obscures the detailed study of stellar properties such as luminosity and morphology. Some of the identified galaxies have been identified only by nebular emission (such as Ly α , [O III], H α). To detect the stellar continuum from absorbing galaxies unambiguously and to increase the number of identified hosts, we have conducted a deep imaging survey for host galaxies associated with intervening absorbers toward gamma ray burst (GRB) afterglows. Because the GRB afterglow dims on a short timescale, observations in the direction of GRBs several months after their emergence allow for more sensitive searches for absorbing galaxies than do those in the direction of QSOs, for which the contamination from background lights is significant. Many optical spectroscopy observations of GRB afterglows in the hours after their bursts have been performed to date. Some of these have shown signs of intervening ($z_{\text{abs}} < z_{\text{GRB}}$) absorbers (e.g., Metzger et al. 1997; Mirabal et al. 2002; Vreeswijk et al. 2004; Chen et al. 2005). Several attempts have been made to identify the galaxies giving rise to the intervening absorption systems in the direction of the GRB afterglow. Some of these have successfully identified the galaxies associated with DLAs or metal-absorption systems at $z \sim 1$ (Vreeswijk et al. 2003; Pollack et al. 2009).

In this context, GRB 050730 is a very unique target that has intervening DLA features at $z > 2$, where the discovery rate for identifying the DLA host galaxies toward QSOs is quite low. GRB 050730 was first detected by the *Swift* satellite (Holland et al. 2005) on 2005 July 30. Chen et al. (2005) performed high-resolution ($\sim 10 \text{ km s}^{-1}$) echelle spectroscopy of GRB 050730 4 hr after the initial burst, when the afterglow was bright at $R \sim 17.7$, and confirmed the redshift of its host galaxy at $z_{\text{GRB}} = 3.969$ based on a strong DLA feature ($\log N_{\text{HI}} \sim 22.15$). Additionally, the authors also identified four other intervening absorption systems (Prochaska et al. 2007a): $z_{\text{abs}} = 3.564$ DLA system ($\log N(\text{H I}) \sim 20.3$), $z_{\text{abs}} = 3.022$ sub-DLA system ($\log N(\text{H I}) \sim 19.9$), and $z_{\text{abs}} = 1.773, 2.253$ strong Mg II absorption systems, whose rest-frame equivalent widths ($W_r^{\lambda 2796}$) were $\sim 1 \text{ \AA}$. Chen et al. (2005) estimated the metallicities for the intervening DLA and sub-DLA systems at $z = 3.564$ and 3.022 in terms of silicon abundance using one of the unsaturated Si II absorption lines associated with the each system. They found that both of the intervening DLA and sub-DLA systems show low-metallicities with $[\text{Si}/\text{H}] < -1.3$ and -1.5 ± 0.2 , respectively, which are typical for $z \sim 3$ DLAs (e.g., Fynbo et al. 2008). Strong Mg II absorption systems ($W_r^{\lambda 2796} > 0.3 \text{ \AA}$) are often found to be associated with DLA or Lyman-limit systems ($\log N(\text{H I}) > 17.7$; e.g., Churchill et al. 2000; Rao et al. 2006) and are known to be a strong probe of the intergalactic medium along the line of sight toward QSOs or GRBs. Therefore, deep imaging of the field around GRB 050730 is particularly important for detecting or constraining the stellar

properties of the intervening DLAs or Mg II absorption systems at $z > 2$ for the first time.

In this paper, we present the results of optical to near-infrared deep imaging observations of the field around GRB 050730. The layout of the paper is as follows: the optical and near-infrared observations and data analysis are presented in Section 2. In Section 3, we provide the results of our spectral energy distribution fitting analysis and discuss the properties of the intervening absorbers toward GRB 050730. Our main results are summarized in Section 4. In this paper, we adopt a Λ CDM cosmology with $\Omega_{\Lambda} = 0.7$, $\Omega_M = 0.3$ and $H_0 = 70 \text{ km s}^{-1} \text{ Mpc}^{-1}$.

2. OBSERVATIONS AND RESULTS

2.1. Optical and Near-infrared Imaging

We observed the field around GRB 050730 in 2007 May and June using the Multi-Object InfraRed Camera and Spectrograph (MOIRCS; Suzuki et al. 2008) mounted on the Cassegrain focus of the Subaru telescope at Mauna Kea, Hawaii. We took images in the J and K_s bands, with total exposure times of 3600 and 11160 s, respectively. Seeing sizes were roughly $0''.51$ in the J band and $0''.58$ in the K_s band. A standard star (FS136; Leggett et al. 2006) was observed for flux calibration at the beginning or end of each observation. The data were reduced using a purpose-built pipeline software package called MCSRED (Tanaka et al. 2011). First, we performed flat fielding with self-flat frames made from the actual science images, and then we subtracted the sky background from each image. Finally, the data were co-registered and combined.

We also obtained B -, R_c -, and z' -band optical images of the GRB 050730 field using SuprimeCam (Miyazaki et al. 2002) mounted at the prime focus of the Subaru telescope. The total exposure times for B , R_c , and z' bands were 1950, 4000, and 2530 s, respectively. The seeing size varied between $1''.2$ and $1''.5$ throughout the night of the observations. The data were reduced with standard procedures (i.e., dark and bias subtraction, flat fielding and sky subtraction, distortion correction, point-spread function (PSF) matching, and mosaicking) using the SDFRED package (Yagi et al. 2002; Ouchi et al. 2004). The images were calibrated with observations of the SA104 standard stars (Landolt 2009) at an airmass similar to the observations of the GRB 050730 field.

2.2. Optical and Mid-infrared Archived Images

The field around GRB 050730 was imaged with several telescopes to detect its optical afterglow just after the burst (e.g., Pandey et al. 2006). Moreover, subsequent follow-up deep imaging surveys to detect its host galaxy were made more than several months after the burst when the optical afterglow has disappeared (Chen et al. 2009). We used the archived images to specify the position of the afterglow of GRB 050730 and to provide additional leverage to identify the candidate of the galaxy associated with intervening absorbers.

We used the R -band snapshot images of the field around GRB 050730 observed on 2007 July 30 (just after the burst), with Very Large Telescope (VLT)/FORs2, obtained from the ESO archive. We also used the VLT/FORS2 R and I -band deep imaging data observed in 2008 February–May (more than six months after the burst; i.e., no afterglow in the image). The total exposure times of the deep imaging data are

Table 1
Summary of the Observations and Data.

Band	Instrument	Date	Exp. Time (s)	Seeing (")	Limiting Magnitude ^a
Subaru imaging					
<i>B</i>	SuprimeCam	2007 Jun. 13	1950	1.6	26.21
<i>V</i>	FOCAS	2010 May 5	180	0.8	25.73
<i>R_c</i>	SuprimeCam	2007 Jun. 13	4150	1.5	26.48
<i>z'</i>	SuprimeCam	2007 Jun. 13	2530	1.5	25.10
<i>J</i>	MOIRCS	2007 Jun. 8	3600	0.5	25.22
<i>K_s</i>	MOIRCS	2007 May 1	11160	0.6	25.04
Imaging data from archive					
<i>R_{special}</i>	FORS2/VLT	2006 Feb.–May	9800	0.7	27.69
<i>I</i>	FORS2/VLT	2006 Feb. 25	600	1.0	24.96
<i>L</i> (3.6μm)	IRAC/ <i>Spitzer</i>	2008, Mar. 11.	6970	1.9	24.65
Subaru spectroscopy					
300B+SY47	FOCAS	2010 May 5	5400	0.7	...

^a All magnitudes are shown as 3σ limiting magnitudes measured in $2 \times$ FWHM apertures. The data were corrected for Galactic extinction (Schlegel et al. 1998).

Table 2
List of the Intervening Absorbers Toward GRB 050730

Type	Redshift	$\log N(\text{H I})$ (cm^{-2})	Mg II $W_r^{\lambda 2796}$ (Å)	[Si/H]	M_{AB}	L/L_* ^a	SFR ($M_{\odot} \text{ yr}^{-1}$)	$\log(M_{\text{stellar}}/M_{\odot})$
DLA	3.564	20.03 ± 0.10	...	< -1.3	> -20.79 (<i>B</i>)	< 0.22	$< 1.62^{\text{b}}, 2.45^{\text{c}}$	$< 9.52^{\text{b}}, < 9.92^{\text{c}}$
sub-DLA	3.022	19.90 ± 0.10	...	-1.5 ± 0.2	> -20.49 (<i>V</i>)	< 0.12	$< 1.24^{\text{b}}, 1.87^{\text{c}}$	$< 9.68^{\text{b}}, < 9.92^{\text{c}}$
Mg II	2.253	...	0.886 ± 0.031	...	> -19.95 (<i>R</i>)	< 0.08	$< 0.75^{\text{b}}, 1.14^{\text{c}}$	$< 9.66^{\text{b}}, < 9.68^{\text{c}}$
Mg II	1.773	...	0.943 ± 0.023	...	> -19.49 (<i>I</i>)	< 0.03	$< 0.49^{\text{b}}, 0.74^{\text{c}}$	$< 9.71^{\text{b}}, < 9.54^{\text{c}}$

^a The 3σ upper limit in the K_s -band image (Table 1), which corresponds to the rest-frame optical at the redshift of the absorbers (*B* for $z = 3.564$, *V* for $z = 3.022$, *R* for $z = 2.253$, and *I* for $z = 1.773$), was used for calculating the upper limit of L/L_* . The L_* magnitudes for *B*, *V*, and *R* bands are drawn from a luminosity function at $2 < z < 3.5$ from Marchesini et al. (2007), and the L_* magnitude for the *I* band is drawn from a luminosity function at $z < 2$ from Ilbert et al. (2005).

^b The case that no counterpart associated with the absorbers is detected in the deepest *R*-band image ($R > 27.14$).

^c The case that the candidate G1 ($R \sim 26.69$) is associated with the absorber at each redshift.

9800 and 600 s in the *R* and *I* band, respectively. A basic calibration including bias subtraction, flat fielding, and sky subtraction was performed on each image using the EsoRex FORS pipeline. The resultant images have seeing sizes of $0.''7$ and $1.''0$ in the *R* and *I* band, respectively.

We also obtained the *L*-band ($3.6\mu\text{m}$) *Spitzer*/IRAC images of the field of GRB 050730 from the *Spitzer* archive (Laskar et al. 2011). The total exposure time was 6970 s. The data were reduced using the standard *Spitzer* Science Center pipeline software, whose outputs are Basic Calibrated Data (BCD) FITS files for each frame. The image mosaics were created from the BCD data using the MOPEX software. The FWHM of the PSF in the final image is estimated to be around $1.''9$.

2.3. Limiting Magnitude

To estimate the limiting magnitude, we derived the 1σ background fluctuation in each band by directly measuring the sky fluxes within $2 \times$ FWHM apertures randomly placed on the images. Table 1 summarizes the 3σ limiting magnitude within a $2 \times$ FWHM diameter aperture and seeing size in each band, as well as the observational information. The limiting magnitudes listed in this table are corrected for Galactic extinction toward the field around GRB 050730 ($A_V = 0.156$; Schlegel et al. 1998). Hereafter, we used the magnitude corrected for Galactic extinction.

The *R*-band image of VLT/FORS2 is the deepest among the obtained images. The limiting magnitude of the *R*-band image is 27.69 (AB), which is more than 1 mag deeper than the

rest. Therefore, we use the *R*-band image for detecting galaxies around GRB 050730. However, we do not use the *R*-band image for deriving the luminosity because the *R*-band corresponds to the rest-frame UV wavelength at the absorbers' redshift ($z > 1.7$), and thus mainly traces the star formation activities in galaxies rather than the stellar properties. The K_s band corresponds to the rest-frame optical band at the absorbers' redshift (*B* for $z_{\text{abs}} = 3.969$ and 3.564 , *V* for $z_{\text{abs}} = 3.022$, *R* for $z_{\text{abs}} = 2.253$, and *I* for $z_{\text{abs}} = 1.773$), and thus traces the long-lived stellar population in the galaxies. Therefore, we used the K_s -band image to obtain the galaxy luminosity or its upper limit. Note that although the *L* ($3.6\mu\text{m}$)-band image also traces the rest-frame optical wavelength at the absorbers' redshift, its limiting magnitude (24.65) is brighter than that of the K_s band (25.04; see Table 1).

We derived the absolute magnitude and luminosity in the rest-frame optical for each absorber's redshift corresponding to the 3σ limiting magnitude in the K_s band (Table 2). The luminosity is expressed in terms of L_* by assuming the L_* magnitude drawn from the rest-frame optical luminosity function at $2 < z < 3.5$ (Marchesini et al. 2007, $M_*(B) = -22.39$ for $z_{\text{abs}} = 3.564$, $M_*(V) = -22.77$ for $z_{\text{abs}} = 3.022$, $M_*(R) = -22.67$ for $z_{\text{abs}} = 2.253$) and at $z < 2$ (Ilbert et al. 2005, $M_*(I) = -23.15$ for $z_{\text{abs}} = 1.773$). We emphasize that the limiting magnitude for our K_s -band image corresponds to a luminosity less than $0.3L_*$ at any absorber's redshift, and we note that we can reach the sensitivity necessary to detect sub- L_* galaxies, which are expected to be major contributors to the DLA cross-section (Okoshi & Nagashima 2005).

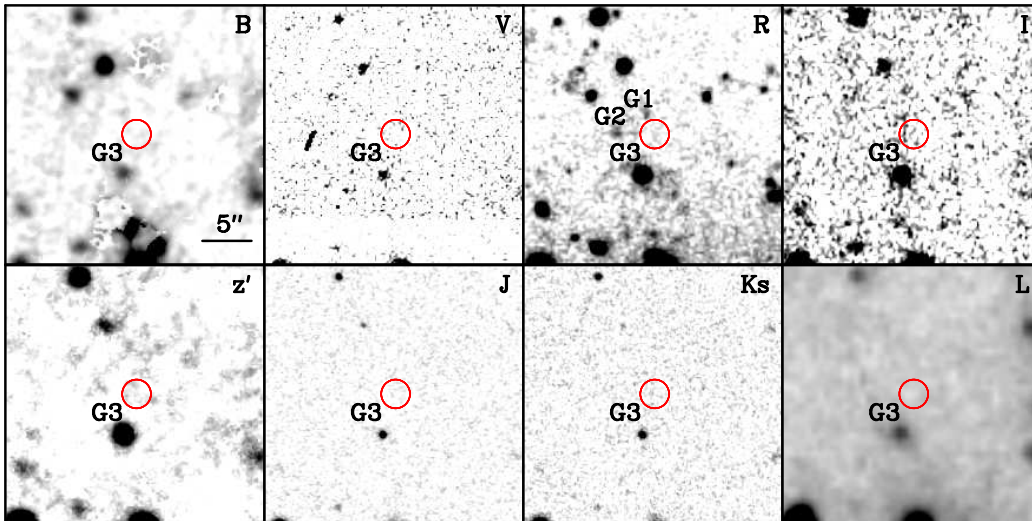


Figure 1. $BVRiz'JK_sL(3.6\mu\text{m})$ -band images of the field around GRB 050730. The size of each panel is $25'' \times 25''$, which corresponds to $\sim 200 \text{ kpc} \times 200 \text{ kpc}$ at the redshift of the intervening absorbers ($z_{\text{abs}} \sim 1.5\text{--}3.5$). North is up, and east is to the left. A red circle in each panel shows the location of the optical afterglow of GRB 050730. The radius of the circle is around 10 kpc at the GRB's redshift ($z = 3.969$), the area in which most GRB host galaxies were discovered (Bloom et al. 2002; Prochaska et al. 2007b). No detectable object is seen within 10 kpc around the GRB afterglow, as reported previously in the literature (Chen et al. 2009).

2.4. Sources around GRB 050730

Figure 1 shows the acquired images of the field around the GRB 050730 afterglow. The size of each panel is $25'' \times 25''$, which roughly covers the area around $\sim 100 \text{ kpc}$ from the line of sight toward the GRB afterglow at the absorbers' redshift ($z_{\text{abs}} \sim 1.7\text{--}3.9$). We detected 27 galaxies within this field of view in the deepest R -band image. Only seven out of the 27 galaxies are detected in the K_s band.

Long-duration GRBs are known to occur exclusively within a few kiloparsecs of the center of star-forming galaxies (Bloom et al. 2002; Fruchter et al. 2006). We confirmed that there was no discernible flux associated with the intrinsic GRB–DLA absorbers at $z \sim 3.968$ within 10 kpc around the afterglow, as already reported in Chen et al. (2009), although our limiting magnitude in R band (~ 27.4) is 1 mag deeper than that of Chen et al. (2009, $R_c \sim 26.4$).

By contrast, intervening DLA or Mg II absorbers are selected independently of any emission or stellar population. Their sight lines are selected by a cross section of the intervening galaxies and should preferentially intersect the outer regions of the interstellar medium in the galaxies. To identify possible candidates for the galaxies associated with the intervening absorbers, we first eliminate galaxies that are located too far away from the line of sight toward the GRB afterglow to produce the observed DLA or Mg II absorptions. We adopted a scaling relation between the galaxy's luminosity (L) and halo radius (R) in the form

$$\frac{R}{R_*} = \left(\frac{L}{L_*} \right)^t \quad (1)$$

to constrain the extension of the gas cloud associated with the DLA or Mg II host galaxies following the method described in Fynbo et al. (1999). In this formula, the halo radius R_* and power-law index t are determined by their fit to the observed DLA or Mg II host galaxies at low redshift ($z < 1$) as $R_* = 42.86 \text{ kpc}$ and $t = 0.26$ for the DLA (Chen & Lanzetta 2003), and $R_* = 107.14 \text{ kpc}$ and $t = 0.35$ for the Mg II system (Chen et al. 2010). Based on the semi-analytic models of galaxy evolution (e.g., Mo et al. 1999), the halo size of galax-

ies is expected to be smaller at higher redshift, which has also been confirmed in several observational studies of disk galaxies (e.g., Barden et al. 2005; Trujillo et al. 2006). Therefore, we used the radius R derived from the above formula as an upper limit of the extension of the gas cloud associated with DLA or Mg II host galaxies at $z \geq 2.0$. Figure 2 shows the apparent separation between the position of 27 detected galaxies in the R band and the position of the afterglow as a function of their apparent magnitude (or 3σ upper limit) in the K_s band, which corresponds to the rest-frame optical band at the redshift of the absorbers. We also plot the upper limits of the halo radii associated with the DLA at $z = 3.564$, sub-DLA at $z = 3.022$, and Mg II system at $z = 2.253$ and 1.773 based on the above formula. The magnitudes corresponding to L_* are drawn from the rest-frame optical luminosity function as in Section 2.3. We found that three galaxies are located below the limit of the halo radius in Figure 2. We identified these three galaxies as candidates for the galaxies associated with the intervening DLA or Mg II absorption systems toward GRB 050730. The three candidates are marked G1, G2, and G3 in Figures 1 and 2 in order of the apparent distance from the position of the afterglow. G1 and G2 are faint and were only detected in the deepest R -band image, whereas G3 is the brightest among the three candidates and was detected in all bands.

2.5. Photometric Color Selection

To further constrain the candidates for the host galaxies of the intervening absorbers, we used the stellar population synthesis models from Bruzual & Charlot (2003) and examined a possible evolutionary track in the two color ($B-R$) versus ($R-K_s$) diagrams at each absorber's redshift (Figure 3). Stellar ages in the tracks range from 1 Myr to the cosmic age at each redshift. Single-stellar population, exponentially decaying star formation with e -folding time τ of 0.05, 0.1, 0.5, and 1 Gyr, and constant star-formation models were used in the evolutionary tracks. We also used two different metallicities, Z_\odot and $1/50 Z_\odot$. We adopted the Salpeter (1955) initial mass function (IMF) with mass cutoffs of 0.1 and $100 M_\odot$ for all cases. No dust attenuation was assumed, as typical DLAs

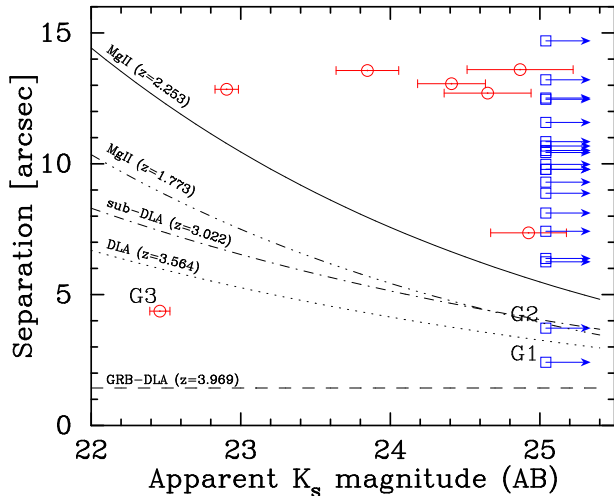


Figure 2. Apparent K_s magnitude vs. separation from the GRB afterglow for galaxies detected within the $25'' \times 25''$ field-of-view around the afterglow. Circles show the galaxies detected in the K_s band. Squares show the galaxies not detected in the K_s band but detected in the R band, and then indicate the 3σ upper limit of the K_s -band magnitude. The dashed line marks the upper limit of the impact parameter (~ 10 kpc) for the host galaxies of GRB 050730 at $z = 3.969$. The triple-dot-dashed line, solid line, dot-dashed line, and dotted line mark the upper limits of the impact parameter of the DLA or Mg II host galaxies at $z = 1.773, 2.253, 3.022,$ and 3.564 , respectively. We estimated the upper limits of the extension of cold gas clouds associated with DLA or Mg II host galaxies using an empirical relation between the galaxy luminosities (L) and radius (R), which is described by a power law of the form $R = 43(L/L_*)^{0.26}$ (kpc) for DLAs (Chen & Lanzetta 2003) and $R = 107(L/L_*)^{0.35}$ (kpc) for Mg II systems (Chen et al. 2010).

show extremely low dust attenuation with $E(B-V) < 0.04$ (e.g., Ellison et al. 2005; Frank & Péroux 2010), and the attenuation should be negligible in this two-color diagram. In Figure 3, we also show the colors for the candidates, G1, G2, and G3. For G1 and G2, because the exact B and K_s magnitudes were not available, we include the possible ranges of color expected from the R -band magnitude and the brightest limit of the B - and K_s -band magnitudes (see Table 1). We found that the color range for G1 (thin gray shaded area in Figure 3) overlaps with any type of evolutionary track at any redshift. The color of G3 (circle in Figure 3) can also be explained by the SED expected from the single stellar population tracks at $z = 3.022$ and $z = 3.564$. These indicate that G1 could be a candidate for the galaxy associated with one of the four intervening absorbers, and G3 could be a candidate for the galaxy associated with either $z = 3.022$ (sub-DLA) or $z = 3.564$ (DLA) intervening absorbers. The color range for G2 (thick gray-shaded area in Figure 3) overlaps with the evolutionary tracks at $z = 3.564$ and marginally overlaps with single stellar population tracks at $z = 3.022$ at an age of around 40 Myr. This also indicates that G2 could be a candidate for the galaxy associated with either of the intervening absorbers at $z = 3.022$ (sub-DLA) or 3.564 (DLA). However, the impact parameter of G2 is larger than the size limit for $z = 3.564$ DLA and too close to the size limit for $z = 3.022$ sub-DLA. Thus, G2 is unlikely to be a galaxy associated with the intervening DLA or Mg II absorption systems toward GRB 050730.

2.6. Spectroscopy of the Brightest Candidate

To identify the redshift of the brightest object (G3), we performed optical spectroscopy with FOCAS mounted on the Cassegrain focus of the Subaru telescope (Kashikawa et al. 2002). We used a $0''.8$ slit, 300B prism, and SY47 order-sort filter, which provided a wavelength coverage of 4800–9000 Å

with a spectral resolution of $\simeq 9.6$ Å, to identify the rest-frame UV spectral features of the absorbers at $z = 2.0$ – 3.5 , such as Ly α emission, continuum depression near the Lyman limit, and several interstellar absorption features seen in the spectra of LBGs (Shapley et al. 2003). During target acquisition, we also took a V -band snapshot image of the field around GRB 050730, including the three candidates, using FOCAS (see Table 1). The total exposure times were 5400 s and 180 s for spectroscopy and snapshot imaging, respectively. Flux calibration and atmospheric absorption-band correction were performed using the spectrum of the spectrophotometric standard star GD153, obtained on the same night. The spectroscopic data were reduced in the standard manner using IRAF. We performed bias subtraction, overscan subtraction, flat fielding with a dome lamp flat, image distortion correction, wavelength calibration with a ThAr lamp, background subtraction, and sky background subtraction. Finally, the two-dimensional spectra were co-registered and combined, and then the one-dimensional spectrum of the object was extracted from the combined two-dimensional spectrum. In Figure 4, we show the resultant FOCAS spectrum of G3. We found no obvious rest-frame UV features in the obtained spectrum.

To further constrain the redshift of G3, we also estimated the photometric redshift of the galaxy based on the photometry in $B, V, R, I, z', J, K_s,$ and $L(3.6\mu\text{m})$ bands (points in Figure 4) using the publicly available software EAZY (Brammer et al. 2008). EAZY fits the observed SED of the galaxy with a combination of galaxy templates. We used the default EAZY template set `eazy_v1.0`, which consists of five templates that span the colors of galaxies in the semi-analytic model and an additional template to compensate for the lack of young and dusty galaxies in the semi-analytic model. Figure 4 shows the best-fit SED template, which is in good agreement with both the photometric points and the observed spectrum. The redshift of the best-fit SED is $z_{\text{phot}} = 0.519^{+0.042}_{-0.028}$. We also show the resulting χ^2 as a function of the photometric redshift, which reaches a minimum at the redshift of the best-fit template ($z_{\text{phot}} = 0.519$). Therefore, we conclude that G3 is most likely at $z \sim 0.5$ and is not related to the known intervening absorbers.

3. CONSTRAINING THE PROPERTIES OF INTERVENING ABSORBERS

The above arguments suggest that G1 is most likely to be a host galaxy of one of the intervening absorbers toward GRB 050730, whereas G2 and G3 are unlikely to be related to the absorbers. In this section, we constrained the SFR and stellar mass for the four intervening absorbers at $z = 1.7$ – 3.5 toward GRB 050730 by assuming that (1) G1 is a host galaxy of the absorber at each redshift or (2) there is no detectable galaxy related to the absorbers. Finally, we compared the constrained SFR and stellar mass of the intervening absorbers at $z = 1.7$ – 3.5 with the other high- z ($z > 2$) galaxy populations.

3.1. Star Formation Rate

We estimated SFRs of the galaxies associated with the intervening DLA or Mg II absorption systems at $z = 1.773, 2.253, 3.022,$ and 3.564 from the rest-frame UV continuum (R -band in the observed frame). We used the empirical formulae of Madau et al. (1998) assuming Salpeter (1955) IMF and no reddening. In Table 2, we show the SFR for the absorbing galaxy at each redshift in case (1), the case that G1 is a host galaxy of the absorbers. We also estimated the SFR using the $3\text{-}\sigma$ upper limit of the rest-frame UV continuum in

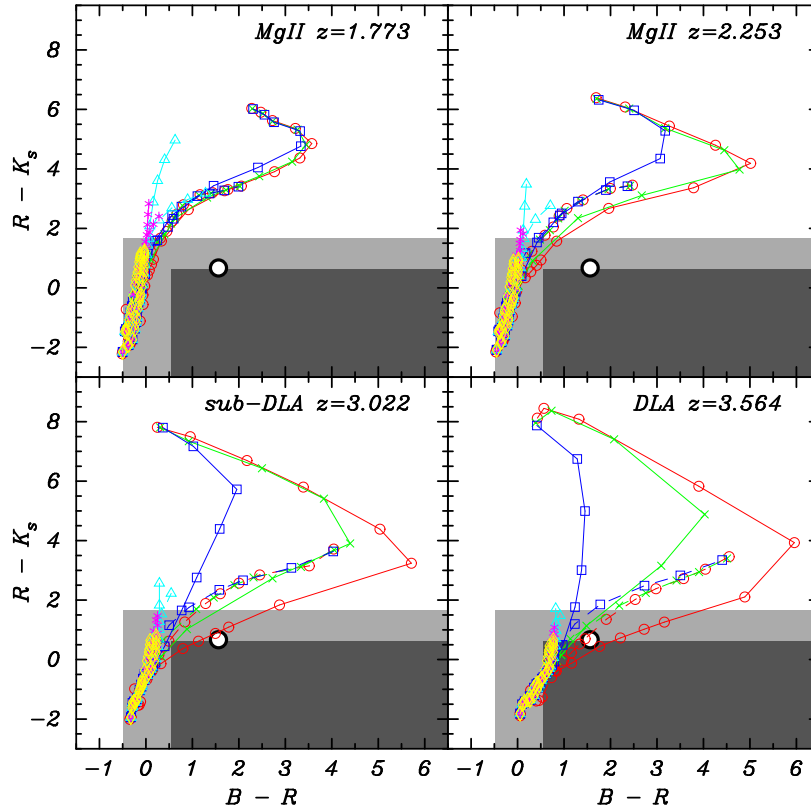


Figure 3. Evolutionary tracks in the two-color ($B-R$) vs. ($R-K_s$) diagrams at the redshift of the intervening absorbers from Bruzual & Charlot (2003) stellar population synthesis models. Stellar ages in the tracks range from 1 Myr to the cosmic age at each redshift. Single-stellar population (circles), exponentially decaying star formation with e -folding time τ of 0.05, 0.1, 0.5, and 1 Gyr (crosses, boxes, triangles, and asterisks, respectively) and constant star formation (diamonds) models are used in these tracks. No dust attenuation is assumed. The solid and dashed lines show the evolutionary tracks for metallicities of Z_\odot and $1/50 Z_\odot$, respectively. Thin and thick gray shaded areas show the range of color expected from the 3σ upper limit of B - and K_s -band magnitudes (see Table 1) and the R -band magnitude of the candidate G1 ($R \sim 26.69$) and G2 ($R \sim 25.65$), respectively. The thick open circle shows the color of candidate 3.

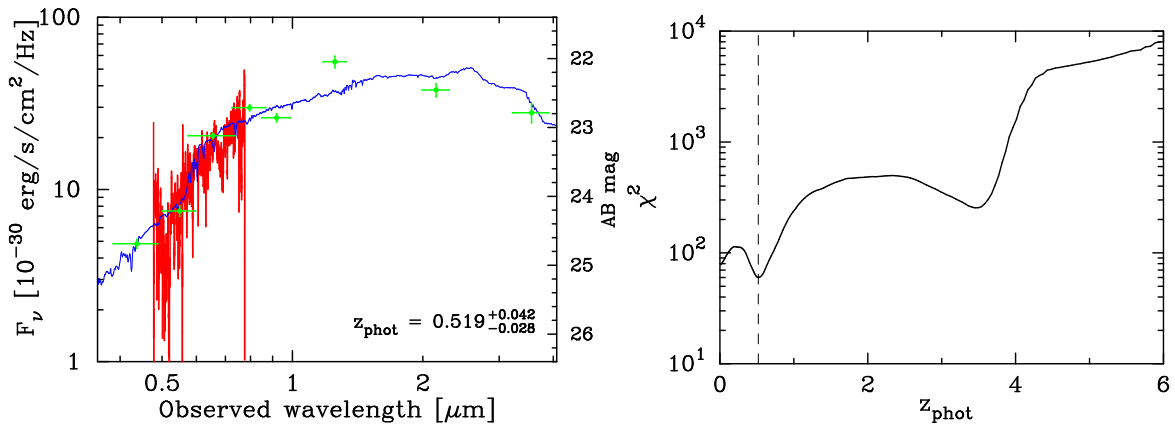


Figure 4. Left: photometric measurements of the candidate G3 (circles with error bars) and the best-fit SED (thin line) to the photometry data. The optical spectrum obtained by FOCAS is also plotted (thick line). The candidate G3 is most likely a low-redshift galaxy at $z \sim 0.5$. Right: χ^2 value of the SED fitting as a function of the photometric redshift.

case (2), the case that there is no galaxy associated with the absorbers. In all cases, we found that the SFR for the DLA galaxies at $z > 3$ was $\sim 2.5 M_\odot \text{ yr}^{-1}$ or smaller. At $z > 2$, Péroux et al. (2012) reported the upper limit of the SFR for typical less metal-rich DLA host galaxies ($Z \leq 0.1 Z_\odot$), which are similar in metallicity to our DLA ($z = 3.564$) and sub-DLA ($z = 3.022$) samples, using the upper limit of the $H\alpha$ fluxes derived from the VLT/SINFONI IFU data. Our derived upper limit for less metal-rich DLA host galaxies is comparable to,

or even more stringent than, that constrained by Péroux et al. (2012, $\sim 3.6 M_\odot \text{ yr}^{-1}$ assuming Salpeter IMF).

In the case of $z \sim 2$ Mg II system ($W_r^{\lambda 2796} \sim 1 \text{ \AA}$), we reached an SFR upper limit of $1.0 M_\odot \text{ yr}^{-1}$, but no host galaxies were clearly detected. By contrast, host galaxies of strong Mg II systems ($W_r^{\lambda 2796} > 0.3 \text{ \AA}$) at $z \sim 1$ were detected with an SFR of more than $10 M_\odot \text{ yr}^{-1}$ (Lovegrove & Simcoe 2011). This difference in the SFR between $z \sim 1$ and $z \sim 2$ was also argued in Bouché et al. (2012) for the case of a very strong

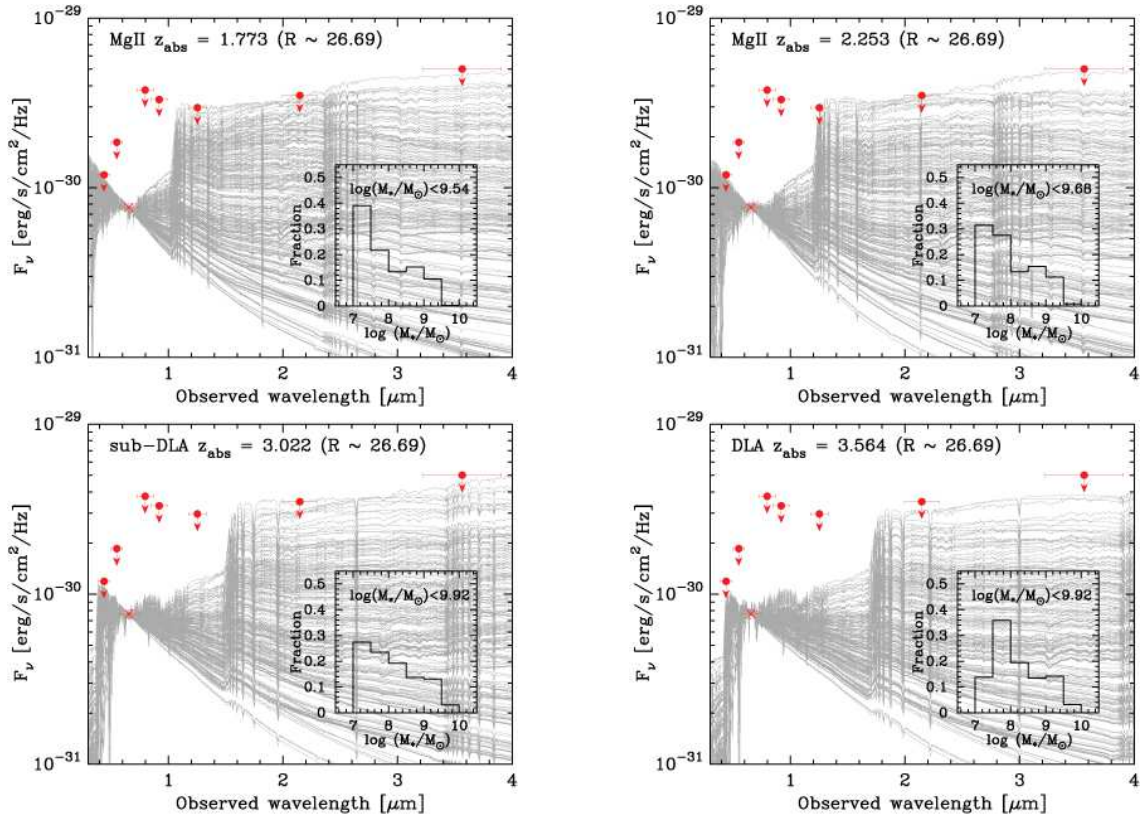


Figure 5. Observed flux of G1 in the R band (cross, $R \sim 26.69$) and the 3σ flux upper limit in $BVIJK,L$ bands (circles, see Table 1) are plotted as a function of the observed wavelength. We fit the model SEDs (solid lines) to the observed flux for the galaxies associated with the intervening DLA or Mg II absorbers at $z \sim 1.773, 2.253, 3.022,$ and 3.564 . The model SEDs were drawn from the stellar population synthesis model of Bruzual & Charlot (2003) by considering a variety of star-formation histories (SFHs) including single-stellar populations, exponentially declining SFRs with e -folding timescales from 10 Myr to 5 Gyr, and constant star formation, and two different metallicities with $Z = Z_{\odot}$ and $0.02Z_{\odot}$. The models were computed for ages from 1 Myr to the cosmic age at each redshift. No dust reddening was assumed in the model SEDs. Fluxes of the model SEDs were scaled to fit the R -band flux of G1 (see the main text for details). Using the scaled flux and mass-luminosity ratio of the model SEDs, we constrained the stellar mass of the intervening DLA or Mg II host galaxies. The inset in each figure shows the distribution of the stellar masses derived from the model SEDs for each intervening absorber.

Mg II system with $W_r^{\lambda 2796} \sim 2.0 \text{ \AA}$. They concluded that $z \sim 2$ Mg II absorbers reside in smaller halos than $z \sim 1$ systems. Although our sample size is only two, our result for the strong Mg II systems with $W_r^{\lambda 2796} \sim 1.0 \text{ \AA}$ supports the scenario proposed in Bouché et al. (2012).

3.2. Stellar Mass

Using the GRB absorbers, we were able to strictly constrain the continuum flux of the intervening absorbers, as the background GRB afterglow used for identifying the absorbers had completely disappeared when we performed the deep imaging. Thus, we did not need to consider the ambiguity of the noise estimation arising from the background PSF subtraction. Moreover, we could eliminate the possibility that the galaxy associated with the absorbers was hidden in the un-subtracted core of the background PSF, even if there was no detectable galaxy around the position of the afterglow. These unambiguous constraints on the continuum level provide a unique opportunity to constrain the stellar mass of DLA or Mg II host galaxies at $z > 2$ for the first time.

The upper limits on the stellar masses associated with the intervening DLA or Mg II absorption systems at $z = 1.773, 2.253, 3.022,$ and 3.564 were derived by fitting the stellar population synthesis models of Bruzual & Charlot (2003) to the upper limit for each object's continuum flux. We used the same set of stellar population synthesis models as were used in Section 2.5. We derived the upper limit of the stellar mass at each redshift for two separate cases: (1) we as-

sumed that G1 was a host galaxy of the absorber, and (2) we assumed that no galaxy was associated with the absorber. Figure 5 shows the fitted model SEDs at each redshift of the intervening absorption systems as a function of the observed wavelength, assuming case (1). In the same figure, we also plot the flux of G1 in the R band and the $3\text{-}\sigma$ upper limits on the fluxes in the other observing bands. In case (1), the model SEDs were scaled to fit the R -band flux of G1. In this case, we excluded any model SEDs whose scaled fluxes exceeded any of the $3\text{-}\sigma$ upper limits for the observed bands other than the R -band. In case (2), the model SEDs were scaled to avoid exceeding any of the $3\text{-}\sigma$ upper limits in the observed bands. Table 2 summarizes the results of the stellar mass estimations. We found that the stellar mass of the DLA or Mg II absorbers at $z \gtrsim 2$ is less than a few times $10^9 M_{\odot}$, which is comparable to the mass of dwarf galaxies like LMC (Harris & Zaritsky 2009).

It should be noted that our derived upper limits on the stellar mass for the less metal-rich DLA at $z = 3.564$ ($[\text{Si}/\text{H}] < -1.3$) and sub-DLA at $z = 3.022$ ($[\text{Si}/\text{H}] = -1.5 \pm 0.2$) are consistent with the stellar masses predicted from the observed mass-metallicity relation for $z > 2$ star-forming galaxies (e.g., Savaglio et al. 2005; Maiolino et al. 2008).

3.3. Comparison with Other $z > 2$ Galaxy Populations

In this section, we compare the measured (or constrained) SFRs and stellar masses for the DLA and Mg II host galaxies at $z_{\text{abs}} \geq 2$ against those obtained for other $z > 2$ galaxy

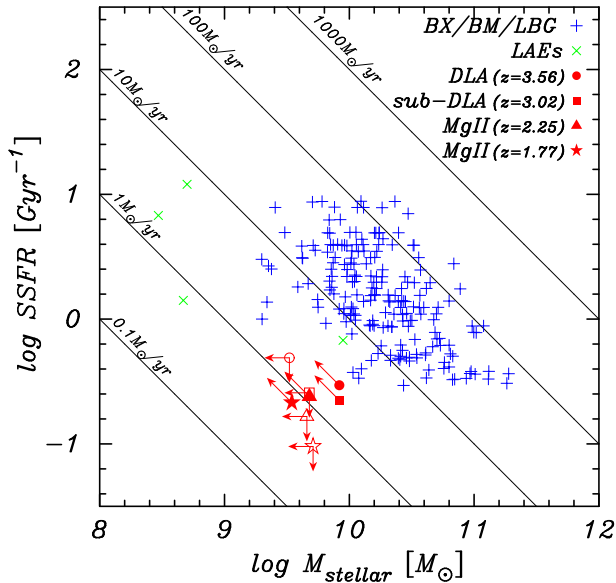


Figure 6. Specific star formation rate (SSFR) as a function of stellar mass for DLA host galaxies at $z = 3.022$ (squares), 3.564 (circles) and Mg II host galaxies at $z = 1.773$ (triangles), 2.253 (stars). In the sample plot, we show the values for LBGs (Reddy et al. 2006; Erb et al. 2006, pluses) and LAEs (Gawiser et al. 2006; Nilsson et al. 2007; Lai et al. 2008, crosses) at $z = 2-3$. Because the candidate of the host galaxy for each absorber is not clearly identified, we plot the SSFRs assuming that G1 is a host galaxy of each absorber (filled symbols) or that no galaxy in our image is associated with any absorber (open symbols). The solid lines show the SSFRs for constant SFRs from 0.1 to $1000 M_{\odot} \text{ yr}^{-1}$.

populations, such as LBGs (e.g., Reddy et al. 2006; Erb et al. 2006) and LAEs (e.g., Gawiser et al. 2006; Nilsson et al. 2007; Lai et al. 2008). To compare the distribution of their SFRs and stellar masses, we investigated their specific star formation rates (SSFRs). The SSFR is defined as the ratio between the SFR and the stellar mass, and it is an indicator of the intensity of star formation in the galaxy. In Figure 6, we plot the SSFR versus stellar mass for our DLA absorbers at $z > 3$ and Mg II absorbers at $z \sim 2$. Given that we do not identify a galaxy corresponding to each absorber, we constrained the SSFR for each absorber in two separate cases: (1) we assumed that G1 was a host galaxy of the absorber, and (2) we assumed that no host galaxy was detected in our image. For all cases, we found that our absorbing galaxies were located between the low mass end of LBGs and LAEs. This implies that our sample absorbers, which consist of less metal-rich ($[\text{Si}/\text{H}] < -1.0$) DLAs and Mg II systems, should not reside in the massive star-forming galaxies (like typical LBGs). Indeed, our derived SSFRs for the DLA/Mg II absorbers are consistent with the SSFRs of $z = 1.7-2.5$, less metal-rich DLAs, as derived from their abundance pattern using star formation histories (SFHs) similar to local irregular or dwarf starburst galaxies with weak star formation efficiency (Dessauges-Zavadsky et al. 2007; Calura et al. 2009).

4. CONCLUSIONS

We analyzed deep imaging data of the field around GRB 050730 in optical to mid-infrared wavelengths to identify the host galaxies giving rise to the intervening DLA and Mg II absorbers at $z = 1.773, 2.253, 3.022$, and 3.564 . We used our own near-infrared and optical imaging data obtained with the Subaru telescope, together with archived optical and mid-infrared imaging data obtained with the VLT and *Spitzer*. We examined the color, impact parameter, and photometric red-

shift (for the brightest galaxy only) for the galaxies detected in our multi-color images to constrain the candidates for the galaxies associated with the intervening absorbers. We found no unambiguous candidate for the host galaxies in our data. Using the 3σ limiting flux or the flux of the marginally detected galaxy (G1) in the *R*-band image (corresponding to the UV wavelength in the rest-frame of the intervening absorbers), we placed the following constraints on the upper limits of the SFR in the galaxies giving rise to the intervening absorbers: $2.5 M_{\odot} \text{ yr}^{-1}$ for the DLA and sub-DLA systems and $1.0 M_{\odot} \text{ yr}^{-1}$ for the Mg II systems. We used the $3-\sigma$ upper limit of the flux in each wavelength to constrain the stellar mass of the absorbing galaxies to be several times $10^9 M_{\odot}$ or lower. We confirmed that the stellar mass limits for the DLA and sub-DLA at $z = 3.564$ and 3.022 are consistent with the stellar masses expected from their metallicity, assuming the mass-metallicity relation observed at $z > 3$ (Maiolino et al. 2008). Both the SFR and the stellar mass for the intervening absorbers show properties similar to dwarf galaxies like the LMC (Harris & Zaritsky 2009). The intervening absorbers in the direction of GRB 050730, which consist of the less metal-rich DLAs and Mg II systems with $W_r^{\lambda 2796} \sim 1.0 \text{ \AA}$, show low SSFRs ($\lesssim 1.0 \text{ Gyr}^{-1}$), which are comparable to LAEs or LBGs at the low-mass end of their mass function. This low SSFR for our intervening absorbers favors the scenario that typical DLAs and Mg II systems with low metallicities are likely to reside in dwarf galaxies, rather than in massive star-forming galaxies like typical LBGs.

We thank Kentaro Aoki and Takuji Tsujimoto for helpful discussions in the early stage of this work and for careful reading of the manuscript. This work is mainly based on data collected with the Subaru Telescope, which is operated by National Astronomical Observatory of Japan (NAOJ). Also, this work is based in part on archival data obtained from the ESO Science Archive Facility and *Spitzer Space Telescope*, which is operated by the Jet Propulsion Laboratory, California Institute of Technology, under a contract with NASA.

REFERENCES

- Barden, M., et al. 2005, *ApJ*, 635, 959
 Bloom, J. S., Kulkarni, S. R., & Djorgovski, S. G. 2002, *AJ*, 123, 1111
 Bouché, N., Murphy, M. T., Péroux, C., et al. 2012, *MNRAS*, 419, 2
 Brammer, G. B., van Dokkum, P. G., & Coppi, P. 2008, *ApJ*, 686, 1503
 Bruzual, G., & Charlot, S. 2003, *MNRAS*, 344, 1000
 Chen, H.-W., & Lanzetta, K. M. 2003, *ApJ*, 597, 706
 Chen, H.-W., Prochaska, J. X., Bloom, J. S., & Thompson, I. B. 2005, *ApJ*, 634, L25
 Chen H. W. et al., 2009, *ApJ*, 691, 152
 Chen, H.-W., Helsby, J. E., Gauthier, J.-R., Shectman, S. A., Thompson, I. B., & Tinker, J. L. 2010, *ApJ*, 714, 1521
 Churchill, C. W., Mellon, R. R., Charlton, J. C., et al. 2000, *ApJS*, 130, 91
 Calura, F., Dessauges-Zavadsky, M., Prochaska, J. X., & Matteucci, F. 2009, *ApJ*, 693, 1236
 Cole, S., Norberg, P., Baugh, C. M., et al. 2001, *MNRAS*, 326, 255
 Cowie, L. L., & Hu, E. M. 1998, *AJ*, 115, 1319
 Dessauges-Zavadsky, M., Calura, F., Prochaska, J. X., D’Odorico, S., & Matteucci, F. 2007, *A&A*, 470, 431
 Ellison, S. L., Hall, P. B., & Lira, P. 2005, *AJ*, 130, 1345
 Erb, D. K., Steidel, C. C., Shapley, A. E., et al. 2006, *ApJ*, 647, 128
 Fall, S. M., & Efstathiou, G. 1980, *MNRAS*, 193, 189
 Frank, S., & Péroux, C. 2010, *MNRAS*, 406, 2235
 Fruchter, A. S., et al. 2006, *Nature*, 441, 463
 Fynbo, J. U., Møller, P., & Warren, S. J. 1999, *MNRAS*, 305, 849
 Fynbo, J. P. U., Prochaska, J. X., Sommer-Larsen, J., Dessauges-Zavadsky, M., & Møller, P. 2008, *ApJ*, 683, 321
 Fynbo, J. P. U., Laursen, P., Ledoux, C., et al. 2010, *MNRAS*, 408, 2128

- Fynbo, J. P. U., Ledoux, C., Noterdaeme, P., et al. 2011, *MNRAS*, 413, 2481
 Gawiser, E., van Dokkum, P. G., Gronwall, C., et al. 2006, *ApJ*, 642, L13
 Harris, J., & Zaritsky, D. 2009, *AJ*, 138, 1243
 Holland, S. T., Barthelmy, S., Burrows, D. N., et al. 2005, *GRB Coordinates Network*, 3704, 1
 Kashikawa, N., et al. 2002, *PASJ*, 54, 819
 Ilbert, O., et al. 2005, *A&A*, 439, 863
 Lai, K., Huang, J.-S., Fazio, G., et al. 2008, *ApJ*, 674, 70
 Landolt, A. U. 2009, *AJ*, 137, 4186
 Laskar, T., Berger, E., & Chary, R.-R. 2011, *ApJ*, 739, 1
 Ledoux, C., Petitjean, P., Fynbo, J. P. U., Møller, P., & Srianand, R. 2006, *A&A*, 457, 71
 Leggett, S. K., et al. 2006, *MNRAS*, 373, 781
 Lovegrove, E., & Simcoe, R. A. 2011, *ApJ*, 740, 30
 Madau, P., Pozzetti, L., & Dickinson, M. 1998, *ApJ*, 498, 106
 Maiolino, R., Nagao, T., Grazian, A., et al. 2008, *A&A*, 488, 463
 Marchesini, D., et al. 2007, *ApJ*, 656, 42
 Metzger, M. R., Djorgovski, S. G., Kulkarni, S. R., et al. 1997, *Nature*, 387, 878
 Miyazaki, S., et al. 2002, *PASJ*, 54, 833
 Mirabal, N., Halpern, J. P., Kulkarni, S. R., et al. 2002, *ApJ*, 578, 818
 Mo, H. J., Mao, S., & White, S. D. M. 1999, *MNRAS*, 304, 175
 Møller, P., Warren, S. J., Fall, S. M., Fynbo, J. U., & Jakobsen, P. 2002, *ApJ*, 574, 51
 Møller, P., Fynbo, J. P. U., & Fall, S. M. 2004, *A&A*, 422, L33
 Nilsson, K. K., Møller, P., Møller, O., et al. 2007, *A&A*, 471, 71
 Noterdaeme, P., Petitjean, P., Ledoux, C., & Srianand, R. 2009, *A&A*, 505, 1087
 Noterdaeme, P., Laursen, P., Petitjean, P., et al. 2012, *A&A*, 540, A63
 Okoshi, K., & Nagashima, M. 2005, *ApJ*, 623, 99
 Ouchi, M., et al. 2004, *ApJ*, 611, 660
 Pandey, S. B., Castro-Tirado, A. J., McBreen, S., et al. 2006, *A&A*, 460, 415
 Péroux, C., McMahon, R. G., Storrie-Lombardi, L. J., & Irwin, M. J. 2003, *MNRAS*, 346, 1103
 Péroux, C., Bouché, N., Kulkarni, V. P., York, D. G., & Vladilo, G. 2012, *MNRAS*, 419, 3060
 Pollack, L. K., Chen, H.-W., Prochaska, J. X., & Bloom, J. S. 2009, *ApJ*, 701, 1605
 Prochaska, J. X., & Wolfe, A. M. 2009, *ApJ*, 696, 1543
 Prochaska, J. X., Chen, H.-W., Bloom, J. S., et al. 2007a, *ApJS*, 168, 231
 Prochaska, J. X., Chen, H.-W., Dessauges-Zavadsky, M., & Bloom, J. S. 2007b, *ApJ*, 666, 267
 Rao, S. M., Belfort-Mihalyi, M., Turnshek, D. A., et al. 2011, *MNRAS*, 416, 1215
 Rao, S. M., Turnshek, D. A., & Nestor, D. B. 2006, *ApJ*, 636, 610
 Rao, S. M., Nestor, D. B., Turnshek, D. A., et al. 2003, *ApJ*, 595, 94
 Reddy, N. A., Steidel, C. C., Fadda, D., et al. 2006, *ApJ*, 644, 792
 Salpeter, E. E. 1955, *ApJ*, 121, 161
 Savaglio, S., Glazebrook, K., Le Borgne, D., et al. 2005, *ApJ*, 635, 260
 Schlegel, D. J., Finkbeiner, D. P., & Davis, M. 1998, *ApJ*, 500, 525
 Shapley, A. E., Steidel, C. C., Pettini, M., & Adelberger, K. L. 2003, *ApJ*, 588, 65
 Steidel, C. C., Adelberger, K. L., Shapley, A. E., et al. 2003, *ApJ*, 592, 728
 Suzuki, R., et al. 2008, *PASJ*, 60, 1347
 Tanaka, I., Breuck, C. D., Kurk, J. D., et al. 2011, *PASJ*, 63, 415
 Trujillo, I., et al. 2006, *ApJ*, 650, 18
 Vreeswijk, P. M., Møller, P., & Fynbo, J. P. U. 2003, *A&A*, 409, L5
 Vreeswijk, P. M., Ellison, S. L., Ledoux, C., et al. 2004, *A&A*, 419, 927
 White, S. D. M., & Rees, M. J. 1978, *MNRAS*, 183, 341
 Wolfe, A. M., Turnshek, D. A., Smith, H. E., & Cohen, R. D. 1986, *ApJS*, 61, 249
 Yagi, M., Kashikawa, N., Sekiguchi, M., Doi, M., Yasuda, N., Shimasaku, K., & Okamura, S. 2002, *AJ*, 123, 66